nature geoscience

ARTICLES

PUBLISHED ONLINE: 21 AUGUST 2017 | DOI: 10.1038/NGEO3012

Anatomy of a meltwater drainage system beneath the ancestral East Antarctic ice sheet

Lauren M. Simkins[1]*, John B. Anderson[1], Sarah L. Greenwood[2], Helge M. Gonnermann[1], Lindsay O. Prothro[1], Anna Ruth W. Halberstadt[1,3], Leigh A. Stearns[4], David Pollard[5] and Robert M. DeConto[3]

Subglacial hydrology is critical to understand the behaviour of ice sheets, yet active meltwater drainage beneath contemporary ice sheets is rarely accessible to direct observation. Using geophysical and sedimentological data from the deglaciated western Ross Sea, we identify a palaeo-subglacial hydrological system active beneath an area formerly covered by the East Antarctic ice sheet. A long channel network repeatedly delivered meltwater to an ice stream grounding line and was a persistent pathway for episodic meltwater drainage events. Embayments within grounding-line landforms coincide with the location of subglacial channels, marking reduced sedimentation and restricted landform growth. Consequently, channelized drainage at the grounding line influenced the degree to which these landforms could provide stability feedbacks to the ice stream. The channel network was connected to upstream subglacial lakes in an area of geologically recent rifting and volcanism, where elevated heat flux would have produced sufficient basal melting to fill the lakes over decades to several centuries; this timescale is consistent with our estimates of the frequency of drainage events at the retreating grounding line. Based on these data, we hypothesize that ice stream dynamics in this region were sensitive to the underlying hydrological system.

Subglacial processes influence the behaviour of ice sheets and their grounding lines, the most downstream location ice sheets are in contact with the underlying bed. In particular, meltwater beneath ice sheets is associated with the onset of fast-flowing ice streams[1], shear margins that separate fast from slow ice flow[2], and enhanced deformation of subglacial sediments[3,4]. Meltwater stored within subglacial lakes[5–7] can drain over periods of months to several years[8–11] due to changes in hydraulic gradient that are probably triggered by ice thinning and grounding-line retreat[10,11]. Downstream of draining subglacial lakes, periods of fluctuating and accelerated ice flow have been interpreted to result from distributed water flow[10,12–14]. In contrast, decelerated ice flow has been attributed to lowered basal water pressures, as a consequence of channelized meltwater drainage[15–17]. The distribution and movement of subglacial meltwater, therefore, must be well understood to assess changes in ice flow, yet models and theory have outpaced our knowledge of subglacial hydrology based on direct observations.

A key question regards the influence of subglacial meltwater drainage on grounding-line dynamics. The termination of a subglacial channel beneath the contemporary Whillans Ice Stream (Fig. 1a) coincides with a grounding-line embayment, where the grounding line is located several kilometres further inland from the adjacent grounding line and sediment erosion within the channel and water mixing may alter grounding-line behaviour[18,19]. Whether a causal relationship exists between channelized drainage and grounding-line embayments is unclear; however, the possibility that channelized drainage influences grounding-line position and sediment accumulation, which can reduce the ice thickness needed to remain in contact with the bed and even facilitate ice advance[20,21], should be explored. Furthermore, subglacial channels draining at the grounding line can release buoyant meltwater plumes that thermally erode channels into the base of ice shelves[22,23]. One such example suggests basal melt rates of $>15\,m\,yr^{-1}$ within an actively forming ice shelf channel that is connected to a hypothesized subglacial channel at the grounding line[24]. Although these observations demonstrate that subglacial channels drain at grounding lines and can cause ice shelf melting, their impact on grounding-line dynamics remains tenuous.

The geologic record can provide broader spatial and temporal perspectives on subglacial hydrology. Numerous palaeo-subglacial channels incised into bedrock are exposed on the Antarctic continental shelf[25–29] (Fig. 1a), but the timing of their incision and meltwater occupation is not well constrained. Surficial sediment-based subglacial channels on the Antarctic continental shelf are temporally constrained[30,31], yet they have not thus far been linked to former grounding lines. Using geophysical and sedimentological data, we provide the first evidence of a subglacial hydrological system that was active during the post-Last Glacial Maximum (LGM) deglaciation and connected explicitly to grounding-line positions of a former ice stream in the western Ross Sea (Fig. 1a).

Channelized drainage at palaeo-grounding-line positions

Multibeam bathymetry data with sub-metre vertical resolution reveal a subglacial hydrological system that spans over 200 km in distance, with cross-cutting relationships between glacial landforms that record post-LGM ice flow and retreat of an ice stream sourced from the East Antarctic ice sheet (EAIS) (Fig. 1b). For a regional-scale reconstruction of ice flow and retreat in the Ross Sea, readers are referred to ref. 32. Grounding-line landforms, including recessional moraines and grounding-zone wedges, represent

[1]Department of Earth, Environment and Planetary Sciences, Rice University, Houston, Texas 77005, USA. [2]Department of Geological Sciences, Stockholm University, Stockholm 10691, Sweden. [3]Department of Geosciences, University of Massachusetts, Amherst, Massachusetts 01003, USA. [4]Department of Geology, University of Kansas, Lawrence, Kansas 66045, USA. [5]Earth and Environmental Systems Institute, Pennsylvania State University, University Park, Pennsylvania 16802, USA. *e-mail: lsimkins@rice.edu

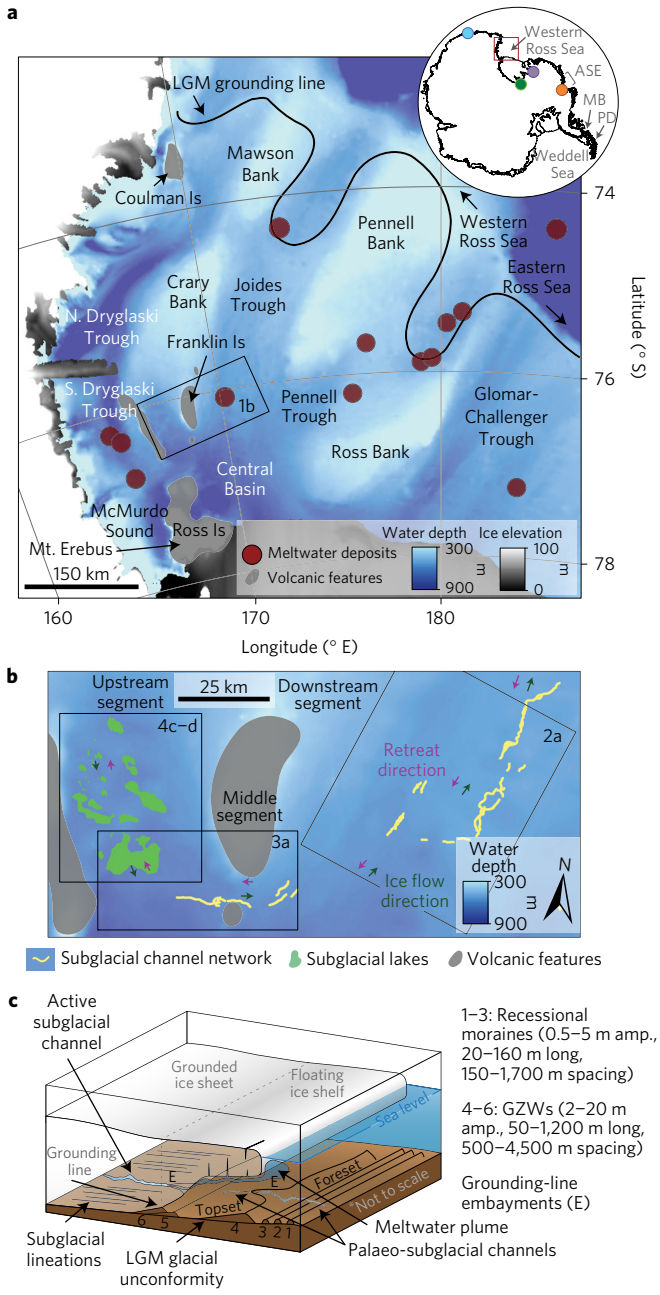

Figure 1 | Western Ross Sea bathymetry and landforms. a, Bathymetry from ref. 49. Ice surface elevation from ref. 50. Inset shows Mertz Trough (blue circle), Whillans (green circle) and MacAyeal (purple circle) ice streams, Pine Island Glacier (orange circle), and palaeo-subglacial channels on the continental shelf. ASE, Amundsen Sea Embayment; MB, Marguerite Bay; PD, Palmer Deep. **b**, Overview of the mapped subglacial hydrological system. **c**, Schematic of the grounding-line environment and landforms. Moraines formed at times 1–3, followed by retreat to new positions at times 4–6 marked by grounding-zone wedges (GZWs). Channelized drainage bisected a moraine at time 2 and produced embayments at times 4 and 6.

periods of grounding-line position stability on the continental shelf (Fig. 1c). Recessional moraines have symmetric geometries and form by sediment deformation and/or deposition at grounding lines[33,34]. Grounding-zone wedges form by sediment delivery from the subglacial environment to marine-based grounding lines and are characterized by asymmetric geometries that result from topset aggradation and foreset progradation[20,33,35,36]. Across the subglacial hydrological system, recessional moraines range in amplitude from 0.5–5 m and grounding-zone wedges are 2–20 m in amplitude (Fig. 1c). We separate the hydrological system into three segments for the purposes of discussion (Fig. 1b): the downstream segment in southern Joides Trough (Fig. 2), the middle segment south of Crary Bank (Fig. 3), and the upstream segment containing a series of subglacial lakes (Fig. 4).

The downstream segment contains a long primary channel, several smaller channels, and a suite of grounding-line landforms (Fig. 2a). The primary channel is locally buried by recessional moraines, which indicates that it initially formed as a subglacial channel prior to southward grounding-line retreat across the area (Fig. 2b). A core collected at the channel base (KC28; Fig. 2a) supports channel incision into till deposited during or following the LGM. The channel bisects several recessional moraines (Fig. 2c), implying meltwater discharge events either caused local incision or restricted the growth of the moraines when the grounding line was positioned at those locations.

Following southward retreat from the positions of the moraines, the grounding line is expressed as a composite grounding-zone wedge (GZW1; 20 m in amplitude) comprised of two stacked grounding-zone wedges with multiple embayments ~1–7 km wide along the topset–foreset break (Fig. 2a). The embayments indicate variability in grounding-line processes that resulted in a sinuous grounding line, in contrast to the earlier formed linear recessional moraines that predominantly overprint the channel to the north. Channels emanate from each embayment, while a 2.5-m-deep subglacial channel occurs on the topset of GZW1 (Fig. 2c,d). The depth of channel incision on the topset of GZW1 is far less than the thickness of till (20 m) that composes the grounding-zone wedge and leads us to suggest that this channel segment was incised either during or following the active growth of GZW1. However, local burial of the channel by till indicates grounding-zone wedge construction was not complete when the channel was active because sediments were later mobilized across segments of the channel (Fig. 2c).

The coincident occurrence of channels and embayments, and the connection of the topset channel to the larger embayment, implies that the embayments were locations of channelized drainage at the grounding line, comparable in scale to the contemporary Whillans grounding-line embayment[18] and perhaps similar to embayments (termed 'breach point' and 'indentation') within grounding-zone wedges in Mertz Trough[37]. The preservation of older recessional moraines at the base of the larger embayment is evidence that the embayments formed by restricted sediment deposition, not erosion, at the grounding line. Contrastingly, we observe grounding-zone wedge lobes that prograded over moraines where channels do not occur (Fig. 2c), indicating ice advance was facilitated during the northward expansion of the grounding-zone wedge. Thus, embayments mark sites where local ice stability, usually enhanced by grounding-zone wedge construction, was reduced, contributing to spatial variability in grounding-line sensitivity to flotation. Instability could have been further enhanced by melting of ice seaward of the grounding line by buoyant meltwater plumes. The apparent bisection of several recessional moraines to the north of GZW1 (Fig. 2c) may be similar, but smaller scale, embayments. Additionally, the superposition of embayments and previously formed subglacial channels indicate preferential drainage pathways spanning prolonged periods of grounding-line recession and landform growth.

After ice decoupled from GZW1, the grounding line retreated southwards to another composite grounding-zone wedge (GZW2) with two more grounding-line embayments (Fig. 2a). The grounding line then retreated 25 km to the south, where the retreat direction shifted from south to west across the middle segment of the subglacial hydrological system (Figs 1b and 3a). A suite of recessional moraines and small (<10 m in amplitude) lineated grounding

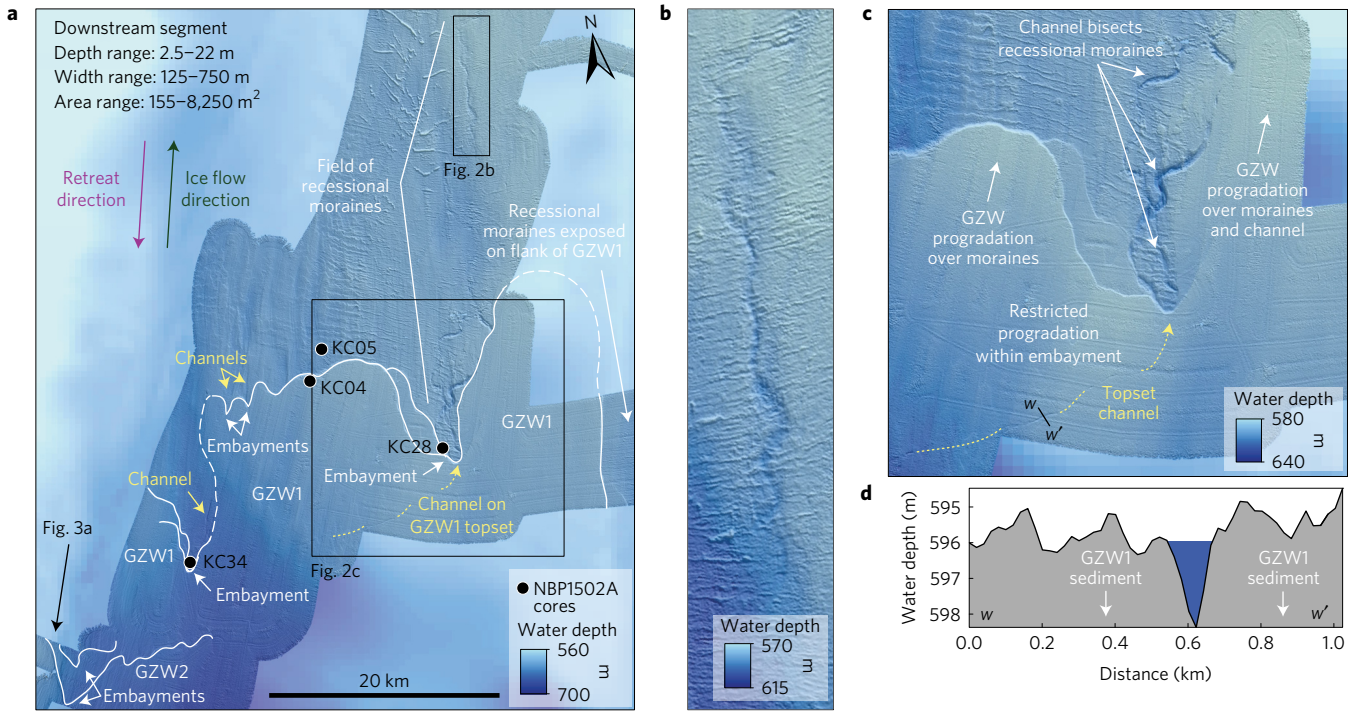

Figure 2 | Downstream hydrological segment. a, One long primary channel, several isolated channels, and grounding-line embayments within composite grounding-zone wedges 1 (GZW1) and 2 (GZW2) in southern Joides Trough (location indicated in Fig. 1b). The topset–foreset breaks of GZW1 and GZW2 are outlined in white. **b**, Channel locally buried by recessional moraines. **c**, A subglacial channel on the topset of GZW1 terminates at the location of the larger grounding-line embayment, flanked by GZW lobes that prograded over recessional moraines. **d**, Profile of shallow channel incised into the topset of GZW1 (location in **c**).

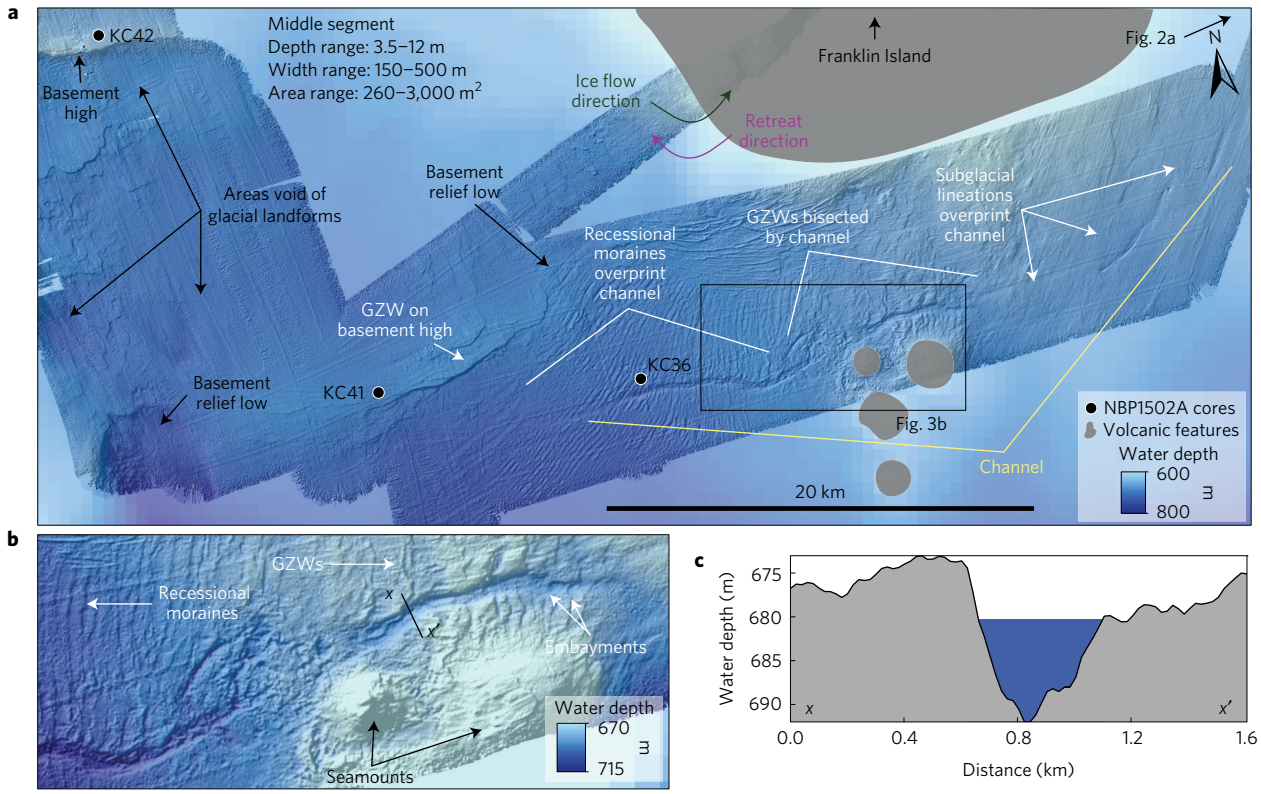

Figure 3 | Middle hydrological segment. a, A single channel is locally buried by recessional moraines and subglacial lineations (location in Fig. 1b). Upstream of the channel to the northwest, smooth areas of the seafloor lack expressions of grounded ice, interpreted as subglacial lakes that delivered meltwater to the channel network through basement relief lows. **b**, Grounding-zone wedges (GZWs) were bisected by the channel as the grounding-line retreated to the west, some of which display small embayments. **c**, Profile across the channel (location in **b**).

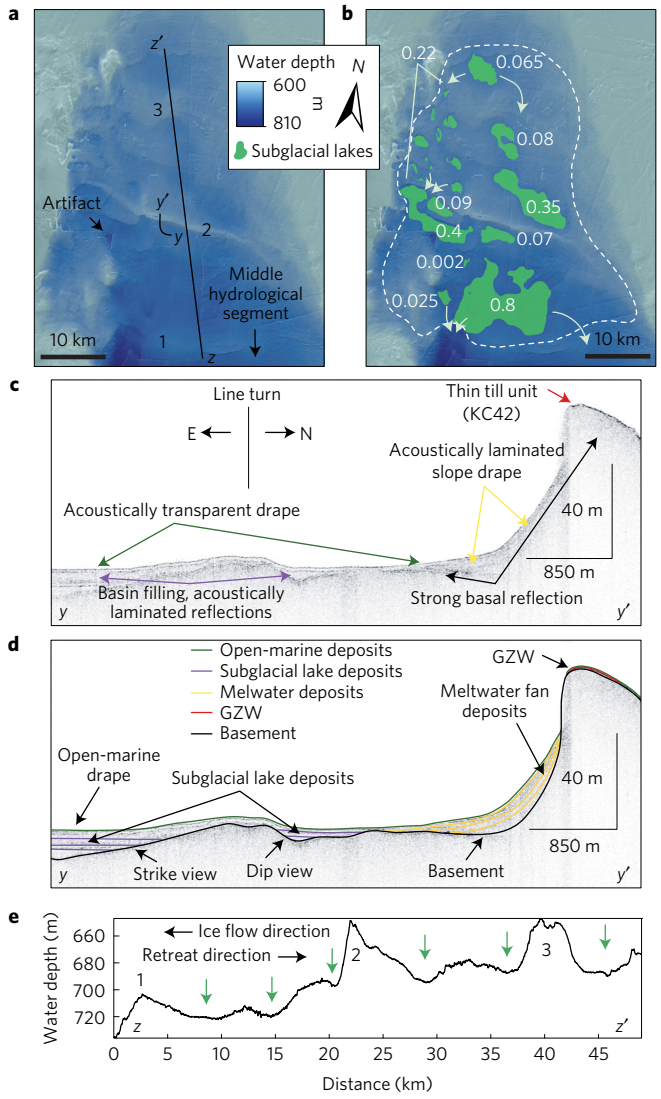

Figure 4 | Subglacial lakes in upstream segment. a, Grounding-line landforms surround basins interpreted as subglacial lakes (location in Fig. 1b). **b**, Same as **a**, but showing identified subglacial lakes (volume capacities in km^3). White arrows show lows in basement relief through which the lakes probably drained. Dashed line denotes the area (1,300 km^2) used to estimate local meltwater production. **c**, Acoustic profile y–y' across a small basin shows a strong basal reflection, two laminated units, and an acoustically transparent unit (location in **a**). **d**, Interpreted acoustic profile shown in **c**. **e**, Profile z–z' across the lakes (location in **a**). Basement highs labelled 1–3.

zone wedges record westward grounding-line retreat, roughly perpendicular to the channel (Fig. 3a). Recessional moraines and subglacial lineations locally overprint the channel (Fig. 3a), which must therefore have been inactive while sediment was mobilized across the channel. In contrast, the channel bisects—or facilitated embayments within—grounding-zone wedges north of the volcanic seamounts (Fig. 3b,c). These variable relationships between the channel and other landforms again indicate episodic meltwater drainage via the channel network during grounding-line retreat.

The spatial association of subglacial channels and former grounding-line positions indicates that the channel network as a whole was a persistent feature during numerous retreat events and periods of ice flow reorganization. Grounding-line landforms that both overprint and were bisected by the channel are oriented perpendicular to the channel, while subglacial lineations are broadly parallel to it. This indicates that ice flow direction and the trajectory of the retreating grounding line maintained a distinct relationship to the established channel network (Fig. 1b), and perhaps indicates sensitivity of ice flow pathways to channelized subglacial drainage, yet we cannot constrain a mechanism for this relationship based on our observations.

Frequency and nature of channelized discharge events

Channelized drainage was predominantly active where grounding-line positions are expressed by grounding-zone wedges and largely dormant during the formation of recessional moraines (Figs 2 and 3). This implies that the frequency of meltwater discharge events typically exceeded the duration of recessional moraine formation and, at most, corresponded to the timing of grounding-zone wedge formation. Grounding-zone wedges several tens to hundreds of metres in amplitude form over centuries to millennia[36,38]. However, using the largest grounding-zone wedge in our study area (GZW1; Figs 1c and 2a,b) and a range of sediment fluxes (Methods), the maximum construction time ranges between 80 and 500 years. Smaller grounding-line landforms bisected by the channel probably formed over years to decades, but we conservatively estimate the frequency of discharge events to decades to several centuries.

We use the smallest channel geometry (Fig. 2d) to provide an estimate of palaeo-meltwater flow conditions, based on a hydropotential surface obtained from palaeo-ice surface and bed elevations (Methods and Supplementary Fig. 1). Calculated bankfull flow velocity is about 1 m s^{-1} with a discharge of 150 m^3 s^{-1}. Given uncertainties in assumptions and modelled parameters to calculate flow properties, these should be treated only as order-of-magnitude estimates. However, the calculated discharge is comparable to peak discharges from contemporary Antarctic subglacial lake drainage events[9,13,39] and meltwater outflow at the Siple Coast grounding line[40].

Sedimentological data help us further characterize the nature of drainage at palaeo-grounding-line positions. Relatively sorted, terrigenous fine silts with little to no biogenic material or ice-rafted debris (Supplementary Fig. 2a–c) occur as discrete units and laminations in sediment cores across the western Ross Sea (Fig. 1a and Supplementary Table 1). Given a shared 10 μm grain-size mode, these deposits were sourced directly from subglacial till (Supplementary Fig. 2d–f). We interpret these as meltwater deposits that were transported by subglacial channels to the grounding line and then dispersed in the ocean before settling to the seafloor. Interestingly, the deposits are identical to meltwater 'plumite' deposits in the Amundsen Sea[41] (Supplementary Fig. 2a) and those described beneath the contemporary Pine Island Glacier ice shelf[42]. In the western Ross Sea, the deposits are confined to proximal grounding line and open marine units, supporting sediment deposition from buoyant meltwater plumes expelled at the grounding line. It is likely that these plumes contributed to melting of ice at the grounding line and to erosion of the ice shelf base.

Upstream subglacial lakes

Within the upstream segment of the subglacial hydrological system (Fig. 1b), we identify a series of subglacial lakes that were dammed by grounded ice (Fig. 4a,b) when the middle and downstream segments of the hydrological system were active. An acoustic profile from this area shows laminated deposits that fill a small basin, stratigraphically bounded by basement rocks and post-LGM open marine deposits and filled with subglacial lake deposits (Fig. 4c,d). Grounding-line landforms surround the basins, but are absent within the basins themselves (Figs 3a and 4a), and indicate another major shift in retreat direction from east to west across the channel to south to north across the subglacial lakes (Figs 1b and 3a). This shows that the grounding-line retreat continued to follow the established subglacial hydrological system.

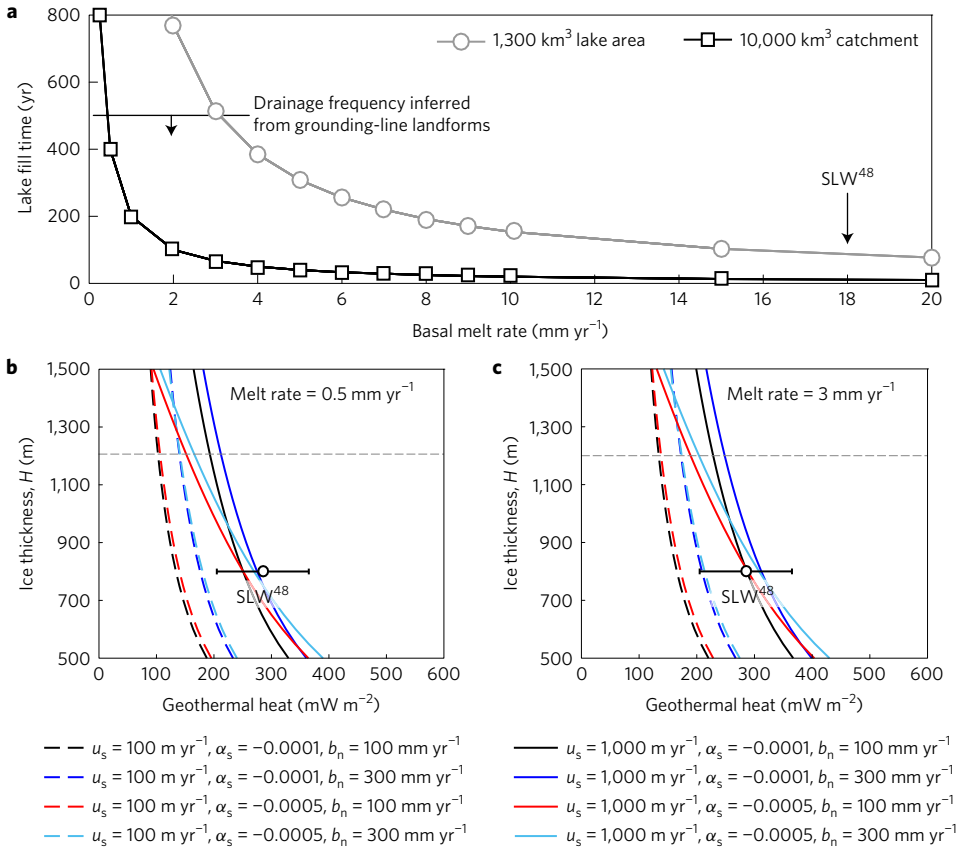

Figure 5 | Conditions required to fill subglacial lakes. a, Timing of lake filling with a range of melt rates across the larger catchment and smaller subglaical lake area, using a 2 km^3 lake volume. **b**,**c**, Geothermal heat flux required to produce melt rates of 0.5 and 3 mm yr^{-1}, respectively, under a range of conditions for ice thickness (H), accumulation rates (b_n), and surface slopes (α_s) and velocities (u_s). Lower (higher) basal melt rates would be achieved by shifting the curves to the left (right) by ~10 mW m^{-2} per 1 mm yr^{-1}. Grey dashed line shows modelled palaeo-ice thickness over the subglacial lakes (Methods). Subglacial Lake Whillans, SLW.

The individual lakes have depths of 4–20 m and volume capacities of 0.002–0.8 km^3 (Fig. 4b); the combined volume capacity is approximately 2 km^3. Although prominent basement highs appear to separate some of the lakes (Fig. 4e), meltwater probably flowed from upstream to downstream subglacial lakes via hydropotential lows and depressions in basement relief (Fig. 4b). This is supported by the presence of meltwater fan deposits on the slope of a basement high at the upstream end of a subglacial lake (Fig. 4a,b), indicating north to south meltwater flow. We suggest that the lakes ultimately drained into the channel system along the southern sill of the largest lake (Figs 3a and 4a,b). If the lakes completely and simultaneously drained, individual channelized drainage events would have lasted about half a year with our calculated channel discharge, or shorter if the lakes did not drain completely or simultaneously.

To what extent the lakes were fed by upstream sources is unclear, as there are no observed channels upstream of the lakes, and distributed drainage is difficult to identify in the geologic record. Distributed sources account for >90% of meltwater stored within contemporary subglacial lakes of the MacAyeal Ice Stream[43] (Fig. 1a). However, it is likely that the drainage catchment for the western Ross Sea lakes was small (<10,000 km^2), since the lakes are perched on the flank of a bank that was a sustained hydropotential high while ice was grounded in this area (Supplementary Fig. 1). If we assume melt across the whole catchment reached and filled these lakes through a distributed drainage system, basal melt rates of >0.5 mm yr^{-1} would be sufficient to produce a lake fill time consistent with the drainage event frequency of at most several centuries inferred from grounding-line landforms (Fig. 5a). Considering the potential absence of significant upstream distributed meltwater sources, an *in situ* basal melt rate of >3 mm yr^{-1} over the area of the subglacial lakes (1,300 km^2; see Fig. 4b) would also produce lake filling on the same timescale (Fig. 5a).

Such rates, under reasonable ice sheet conditions (ice flow velocity, surface slope, accumulation), demand a minimum geothermal heat flux of 90–120 mW m^{-2} (Fig. 5b,c and Supplementary Methods). The subglacial hydrological system is in a region of late Cenozoic rifting[44] and proximal to Quaternary volcanic islands and seamounts[45] (Fig. 1a–b), where measurements of geothermal heat fluxes span from ~60–165 mW m^{-2} (refs 46,47). Along the same rift zone, a heat flux of 285 ± 80 mW m^{-2} was measured at the base of Subglacial Lake Whillans, near the Whillans Ice Stream grounding line (Fig. 1a), with a basal melt rate of ~18 mm yr^{-1} (ref. 48). This melt rate is considerably higher than rates required to fill the western Ross Sea lakes. Therefore, we suggest that elevated, but geologically feasible, geothermal heat fluxes could have produced sufficient basal melting either across the ice stream catchment or confined to the area of the subglacial lakes over periods of decades to several centuries.

Conclusions

An extensive sediment-based subglacial channel network was reactivated numerous times during the post-LGM deglaciation of the western Ross Sea. Channelized meltwater drainage locally restricted grounding-line landform growth and, consequently, contributed to local grounding-line instability. Channel segments both bisect and are buried by grounding-line landforms, suggesting meltwater drainage events occurred episodically, and at periodicities of tens to several hundreds of years. The channel network was fed by upstream

subglacial lakes in an area of geologically recent rifting, active volcanism, and elevated geothermal heat flow. Meltwater drainage configuration appears to have persisted through various phases of grounding-line retreat, shifts in ice flow direction, and a circuitous retreat pattern, suggesting that the stable location of source lakes and ample production of basal melting exerted a degree of influence on the retreating ice stream. The probable recurrence of drainage events during grounding-line landform construction suggests that an individual drainage event is not capable of dislodging a stable grounding line. It does, however, remain a possibility that repeated drainage through embayments, the development of pronounced grounding-line sinuosity and feedbacks with plume-driven ice melting, may undermine grounding-line stability.

Methods

Methods, including statements of data availability and any associated accession codes and references, are available in the online version of this paper.

Received 12 May 2017; accepted 21 July 2017;
published online 21 August 2017

References

1. Peters, L. E., Anandakrishnan, S., Alley, R. B. & Smith, A. M. Extensive storage of basal meltwater in the onset region of a major West Antarctic ice stream. *Geology* **35,** 251–254 (2007).
2. Perol, T., Rice, J. R., Platt, J. D. & Suckale, J. Subglacial hydrology and ice stream margin locations. *J. Geophys. Res.* **120,** 1352–1368 (2015).
3. Alley, R. B., Blankenship, D. D., Bentley, C. R. & Rooney, S. Deformation of till beneath ice stream B, West Antarctica. *Nature* **322,** 57–59 (1986).
4. Engelhardt, H. & Kamb, B. Basal hydraulic system of a West Antarctic ice stream: constraints from borehole observations. *J. Glaciol.* **43,** 207–230 (1997).
5. Palmer, S. J. *et al*. Greenland subglacial lakes detected by radar. *Geophys. Res. Lett.* **40,** 6154–6159 (2013).
6. Howat, I. M., Porter, C., Noh, M. J., Smith, B. E. & Jeong, S. Sudden drainage of a subglacial lake beneath the Greenland Ice Sheet. *Cryosphere* **9,** 103–108 (2015).
7. Wright, A. & Siegert, M. A fourth inventory of Antarctic subglacial lakes. *Antarct. Sci.* **24,** 659–664 (2012).
8. Gray, L. *et al*. Evidence for subglacial water transport in the West Antarctic Ice Sheet through three-dimensional satellite radar interferometry. *Geophys. Res. Lett.* **32,** L03501 (2005).
9. Wingham, D. J., Siegert, M. J., Shepherd, A. & Muir, A. S. Rapid discharge connects Antarctic subglacial lakes. *Nature* **440,** 1033–1036 (2006).
10. Scambos, T. A., Berthier, E. & Shuman, C. A. The triggering of subglacial lake drainage during rapid glacier drawdown: Crane Glacier, Antarctic Peninsula. *Ann. Glaciol.* **52,** 74–82 (2011).
11. Fricker, H. A., Siegfried, M. R., Carter, S. P. & Scambos, T. A. A decade of progress in observing and modeling Antarctic subglacial water systems. *Phil. Trans. R. Soc.* **374,** 20140294 (2016).
12. Bell, R. E., Studinger, M., Shuman, C. A., Fahnestock, M. A. & Joughin, I. Large subglacial lakes in East Antarctica at the onset of fast-flowing ice streams. *Nature* **445,** 904–907 (2007).
13. Stearns, L. A., Smith, B. E. & Hamilton, G. S. Increased flow speed on a large East Antarctic outlet glacier caused by subglacial floods. *Nat. Geosci.* **1,** 827–831 (2008).
14. Siegfried, M. R., Fricker, H. A., Carter, S. P. & Tulaczyk, S. Episodic ice velocity fluctuations triggered by a subglacial flood in West Antarctica. *Geophys. Res. Lett.* **43,** 2640–2648 (2016).
15. Bartholomew, I. *et al*. Seasonal evolution of subglacial drainage and acceleration in a Greenland outlet glacier. *Nat. Geosci.* **3,** 408–411 (2010).
16. Cowton, T. *et al*. Evolution of drainage system morphology at a land-terminating Greenlandic outlet glacier. *J. Geophys. Res.* **118,** 29–41 (2013).
17. Andrews, L. C. *et al*. Direct observations of evolving subglacial drainage beneath the Greenland Ice Sheet. *Nature* **514,** 80–83 (2014).
18. Horgan, H. J. *et al*. Estuaries beneath ice sheets. *Geology* **41,** 1159–1162 (2013).
19. Horgan, H. J., Christianson, K., Jacobel, R. W., Anandakrishnan, S. & Alley, R. B. Sediment deposition at the modern grounding zone of Whillans Ice Stream, West Antarctica. *Geophys. Res. Lett.* **40,** 3934–3939 (2013).
20. Alley, R. B., Anandakrishnan, S., Dupont, T. K., Parizek, B. R. & Pollard, D. Effect of sedimentation on ice-sheet grounding-line stability. *Science* **315,** 1838–1841 (2007).
21. Christianson, K. *et al*. Basal conditions at the grounding zone of Whillans Ice Stream, West Antarctica, from ice-penetrating radar. *J. Geophys. Res.* **121,** 1954–1983 (2016).
22. Le Brocq, A. M. *et al*. Evidence from ice shelves for channelized meltwater flow beneath the Antarctic Ice Sheet. *Nat. Geosci.* **6,** 945–948 (2013).
23. Alley, K. E., Scambos, T. A., Siegfried, M. R. & Fricker, H. A. Impacts of warm water on Antarctic ice shelf stability through basal channel formation. *Nature Geosci.* **9,** 290–293 (2016).
24. Marsh, O. J. *et al*. High basal melting forming a channel at the grounding line of Ross Ice Shelf, Antarctica. *Geophys. Res. Lett.* **43,** 250–255 (2016).
25. Lowe, A. L. & Anderson, J. B. Evidence for abundant subglacial meltwater beneath the paleo-ice sheet in Pine Island Bay, Antarctica. *J. Glaciol.* **49,** 125–138 (2003).
26. Nitsche, F. O. *et al*. Paleo ice flow and subglacial meltwater dynamics in Pine Island Bay, West Antarctica. *Cryosphere* **7,** 249–262 (2013).
27. Anderson, J. B. & Fretwell, L. O. Geomorphology of the onset area of a paleo-ice stream, Marguerite Bay, Antarctic Peninsula. *Earth Surf. Process. Landf.* **33,** 503–512 (2008).
28. Domack, E. *et al*. Subglacial morphology and glacial evolution of the Palmer deep outlet system, Antarctic Peninsula. *Geomorphology* **75,** 125–142 (2006).
29. Campo, J., Wellner, J. S., Lavoie, C., Domack, E. & Yoo, K. C. Glacial geomorphology of the northwestern Weddell Sea, Eastern Antarctic Peninsula Continental Shelf: shifting ice flow patterns during deglaciation. *Geomorphology* **280,** 89–107 (2017).
30. Wellner, J. S., Heroy, D. C. & Anderson, J. B. The death mask of the Antarctic ice sheet: comparison of glacial geomorphic features across the continental shelf. *Geomorphology* **75,** 157–171 (2006).
31. Greenwood, S. L., Gyllencreutz, R., Jakobsson, M. & Anderson, J. B. Ice-flow switching and East/West Antarctic Ice Sheet roles in glaciation of the Western Ross Sea. *Geol. Soc. Am. Bull.* **124,** 1736–1749 (2012).
32. Halberstadt, A. R. W., Simkins, L. M., Greenwood, S. L. & Anderson, J. B. Paleo-ice sheet behaviour: retreat scenarios and changing controls in the Ross Sea, Antarctica. *Cryosphere* **10,** 1003–1020 (2016).
33. Batchelor, C. L. & Dowdeswell, J. A. Ice-sheet grounding-zone wedges (GZWs) on high-latitude continental margins. *Mar. Geol.* **363,** 65–92 (2015).
34. Bouvier, V., Johnson, M. D. & Påsse, T. Distribution, genesis and annual-origin of De Geer moraines in Sweden: insights revealed by LiDAR. *GFF* **137,** 319–333 (2015).
35. Anderson, J. B. *Antarctic Marine Geology* (Cambridge Univ. Press, 1999).
36. Dowdeswell, J. A., Ottesen, D., Evans, J., Cofaigh, C.Ó. & Anderson, J. B. Submarine glacial landforms and rates of ice-stream collapse. *Geology* **36,** 819–822 (2008).
37. McMullen, K. *et al*. Glacial morphology and sediment formation in the Mertz Trough, East Antarctica. *Palaeogeogr. Palaeoclimatol. Palaeoecol.* **231,** 169–180 (2006).
38. Bart, P. J. & Owolana, B. On the duration of West Antarctic Ice Sheet grounding events in Ross Sea during the Quaternary. *Quat. Sci. Rev.* **47,** 101–115 (2012).
39. Smith, B. E., Fricker, H. A., Joughin, I. R. & Tulaczyk, S. An inventory of active subglacial lakes in Antarctica detected by ICESat (2003–2008). *J. Glaciol.* **55,** 573–595 (2009).
40. Carter, S. P. & Fricker, H. A. The supply of subglacial meltwater to the grounding line of the Siple Coast, West Antarctica. *Ann. of Glaciol.* **53,** 267–280 (2012).
41. Witus, A. E. *et al*. Meltwater intensive glacial retreat in polar environments and investigation of associated sediments: example from Pine Island Bay, West Antarctica. *Quat. Sci. Rev.* **85,** 99–118 (2014).
42. Smith, J. A. *et al*. Sub-ice-shelf sediments record history of twentieth-century retreat of Pine Island Glacier. *Nature* **541,** 77–80 (2017).
43. Carter, S. P. *et al*. Modeling 5 years of subglacial lake activity in the MacAyeal Ice Stream (Antarctica) catchment through assimilation of ICESat laser altimetry. *J. Glaciol.* **57,** 1098–1112 (2011).
44. Cooper, A. K., Davey, F. J. & Behrendt, J. C. *The Antarctic Continental Margin: Geology and Geophysics of the Western Ross Sea* Vol. 5B9, 27–65 (Earth Science Series, Circum-Pacific Council for Energy and Mineral Resources, 1987).
45. Rilling, S., Mukasa, S., Wilson, T., Lawver, L. & Hall, C. New determinations of $^{40}Ar/^{39}Ar$ isotopic ages and flow volumes for Cenozoic volcanism in the Terror Rift, Ross Sea, Antarctica. *J. Geophys. Res.* **114,** B12207 (2009).
46. Blackman, D. K., Von Herzen, R. P. & Lawver, L. A. *The Antarctic Continental Margin: Geology and Geophysics of the Western Ross Sea* Vol. 5B, 179–189 (Earth Science Series, Circum-Pacific Council for Energy and Mineral Resources, 1987).
47. Morin, R. H. *et al*. Heat flow and hydrologic characteristics at the AND-1B borehole, ANDRILL McMurdo Ice Shelf Project, Antarctica. *Geosphere* **6,** 370–378 (2010).
48. Fisher, A. T., Mankoff, K. D., Tulaczyk, S. M., Tyler, S. W. & Foley, N. High geothermal heat flux measured below the West Antarctic Ice Sheet. *Sci. Adv.* **1,** 1500093 (2015).

49. Arndt, J. E. *et al*. The international bathymetric chart of the Southern Ocean (IBCSO) Version 1.0—a new bathymetric compilation covering circum-Antarctic waters. *Geophys. Res. Lett.* **40,** 3111–3117 (2013).
50. Fretwell, P. *et al*. Bedmap2: improved ice bed, surface and thickness datasets for Antarctica. *Cryosphere* **7,** 375–393 (2013).

Acknowledgements

The authors thank J. Walder, S. Carter, C. Clark and T. Swanson for productive discussions; B. Demet for assistance in data collection; and A. Fonseca, S. Rezvanbehbahani and J. Aroom for assisting with analyses. This project was supported by the National Science Foundation (NSF-PLR 1246353, J.B.A.) and the Swedish Research Council (D0567301, S.L.G.).

Author contributions

L.M.S. and J.B.A. conceived the research. L.M.S., J.B.A., S.L.G., L.O.P. and A.R.W.H. interpreted the geophysical data. L.M.S. and A.R.W.H. calculated channel flow properties. L.A.S. calculated hydraulic pressure. L.M.S. and L.O.P. analysed sediment samples. D.P. and R.M.D. provided ice sheet model data. H.M.G. completed the heat flow model. L.M.S. wrote the manuscript, with major contributions from J.B.A., S.L.G. and H.M.G. All authors read and commented on the manuscript.

Additional information

Supplementary information is available in the online version of the paper. Reprints and permissions information is available online at www.nature.com/reprints. Publisher's note: Springer Nature remains neutral with regard to jurisdictional claims in published maps and institutional affiliations. Correspondence and requests for materials should be addressed to L.M.S.

Competing financial interests

The authors declare no competing financial interests.

Methods

Bathymetry and acoustic stratigraphy. Multibeam bathymetry was collected on cruise NBP1502A aboard the RVIB *Nathaniel B. Palmer* using a Kongsberg EM-122 system in dual swath mode with a 1° × 1° array and 12 kHz frequency. Vertical resolution varies from 0.07 to 0.2% of the water depth[51] and horizontal resolution is approximately 0.02% the water depth. Data are gridded at 20 m. Sub-bottom acoustic data were collected with a Knudsen CHIRP 3260 system during cruise NBP1502A using a frequency of 3.5 kHz and a 0.25 ms pulse width. Two-way travel time was converted to depth using a velocity of 1,500 m s^{-1}.

Grounding-zone wedge formation time. The sediment volume of GZW 1 (Fig. 2a) of 3×10^9 m^3 or 9×10^4 m^3 m^{-1} (metre width) is based on landform area and thickness, measured from multibeam bathymetry and acoustic profiles. Two-way travel times through sediment were converted to depth using an acoustic velocity bracketed by 1,500–1,750 m s^{-1} (refs 52–54). A lower grounding-line sediment flux of 200 m^3 yr^{-1} m^{-1} (metre width) is based on refs 4,38,55 and a higher flux of 1,000 m^3 m^{-1} yr^{-1} is from ref. 51.

Meltwater channel flow calculations. Meltwater flow velocity and discharge were calculated following refs 56,57 and using the smallest measured channel dimensions (Fig. 2d). Hydraulic potential across the channels is based on isostasy-corrected bed and ice surface elevations from an ice sheet model for a model time slice at 20,000 years ago, representative of the LGM ice sheet configuration (Supplementary Fig. 1). Because the ice sheet model timing is poorly constrained during the deglaciation of the continental shelf, we chose to use the best observationally constrained model time slice (at 20,000 years ago) to estimate hydropotential and, thus, channel flow properties that we advise readers to treat as order-of-magnitude estimates. We did, however, evaluate hydropotential surfaces using model outputs from deglacial time slices, and the hydropotential high on Crary Bank remains and hydropotential across the channel increases, which would lead to higher channel flow discharge yet still within the same order of magnitude. Stream bed roughness was estimated with a dimensionless friction parameterization f for turbulent pipe flow[58] by using equations (1) and (2) to simultaneously solve for f and u (depth-averaged flow velocity).

$$f = \frac{8\Phi h}{\rho_w u^2} \tag{1}$$

$$f^{-0.5} = -1.8 \log_{10}\left[\left(\frac{R}{3.7}\right)^{1.11} + \frac{6.9}{\rho_w u h/\nu}\right] \tag{2}$$

where Φ is hydraulic potential gradient, h is the channel depth, ρ_w is the density of fresh water, ν is kinematic viscosity of water, and R is relative roughness

$$R = \frac{D_{90}}{h} \tag{3}$$

in which grain-size diameter at 90% of the distribution (D_{90}; 1.39 × 10^{-4} m) was used as an estimate for equivalent roughness, based on grain-size measurements from Ross Sea till matrix material (Supplementary Fig. 2d). Although till contains larger clasts (for example, granules and pebbles), we assume the abundant fine-grained matrix is more representative for calculating relative roughness at the base of the channel. A value of 0.097 was used for f, which is similar to the commonly applied value of 0.1 (refs 56,57). Discharge was calculated from the resulting flow velocity and a triangular channel cross-sectional area, assuming bank-full conditions and a flat ice base. Lateral variations in meltwater flow velocity due to the channel banks were not considered, as the channels are much wider than deep, and lateral effects are assumed to be minimal.

Ice sheet model. The ice sheet model is described by refs 59–61. It uses hybrid ice dynamical equations with parameterized flux at the grounding line, allowing the realistic simulation of floating ice shelves, ice streams and grounding-line migration in long-term runs. Elevation surfaces are corrected for glacial isostatic adjustment. The simulation used here is from an intermediate model version, similar to that in ref. 60, with the addition of sub-ice ocean melting parameterization depending on proximal 400 m ocean temperatures[61], which in this run were obtained from archived output of the coupled-GCM experiment of ref. 62. The model was run transiently from 50,000 years ago to the present, on a 20 km grid that spans all of Antarctica.

Sedimentological properties. Sediment samples were sieved prior to measurement with a 500-μm sieve and grain sizes were measured with a Malvern 2000 grain-size analyser. The till measurements do not include the coarser grains (granules and pebbles) and represent the matrix grain size. Core details and sample depths are summarized in Supplementary Table 1.

Heat flow model. The conditions required for basal melting were assessed for a range of parameters using a one-dimensional model similar to that of ref. 63. Further details are in the Supplementary Methods.

Data availability. The authors declare that the data supporting the findings of this study are available within the article and its Supplementary Information file. Multibeam bathymetry data used in this study collected aboard cruise NBP1502A are available in an XYZ format from the corresponding author upon request. Sediment samples from cores used in the study are available by request from the Antarctic Core Collection at the Oregon State University Marine and Geology Repository. Raw sedimentological data is available from the corresponding author upon request.

References

51. Jakobsson, M. *et al*. Geological record of ice shelf break-up and grounding line retreat, Pine Island Bay, West Antarctica. *Geology* **39,** 691–694 (2011).
52. O'Regan, M. *et al*. Constraints on the Pleistocene chronology of sediments from the Lomonosov Ridge. *Paleoceanography* **23,** PA1S19 (2008).
53. Anderson, J. B., Jakobsson, M. & Party, O. S. *Oden Southern Ocean 0910 OSO0910 Cruise Report* (University of Stockholm, 2010).
54. Klages, J. P. *et al*. Retreat of the West Antarctic Ice Sheet from the western Amundsen Sea shelf at a pre-or early LGM stage. *Quat. Sci. Rev.* **91,** 1–15 (2014).
55. Anandakrishnan, S., Catania, G. A., Alley, R. B. & Horgan, H. J. Discovery of till deposition at the grounding line of Whillans Ice Stream. *Science* **315,** 1835–1838 (2007).
56. Walder, J. S. & Fowler, A. Channelized subglacial drainage over a deformable bed. *J. Glaciol.* **40,** 3–15 (1994).
57. Ng, F. S. Canals under sediment-based ice sheets. *Ann. Glaciol.* **30,** 146–152 (2000).
58. Haaland, S. E. Simple and explicit formulas for the friction factor in turbulent pipe flow. *J. Fluids Eng.* **105,** 89–90 (1983).
59. Pollard, D. & DeConto, R. M. Modelling West Antarctic ice sheet growth and collapse through the past five million years. *Nature* **458,** 329–332 (2009).
60. Pollard, D. & DeConto, R. M. Description of a hybrid ice sheet-shelf model, and application to Antarctica. *Geosci. Mod. Dev.* **5,** 1273–1295 (2012).
61. Pollard, D., Chang, W., Haran, M., Applegate, P. & DeConto, R. M. Large ensemble modeling of last deglacial retreat of the West Antarctic Ice Sheet: comparison of simple and advanced statistical techniques. *Geosci. Mod. Dev.* **9,** 1697–1723 (2016).
62. Liu, Z. *et al*. Transient simulation of last deglaciation with a new mechanism for Bolling–Allerød warming. *Science* **325,** 310–314 (2009).
63. Budd, W. F., Jenssen, D. & Radok, U. *Derived Physical Characteristics of the Antarctic Ice Sheet* (Australian National Antarctic Expeditions Interim Reports. Series A, Glaciology, no. 120; University of Melbourne, 1971).